Effects of Radar Sampling on Single-Doppler Velocity Signatures of Mesocyclones and Tornadoes

VINCENT T. WOOD AND RODGER A. BROWN

NOAA/Environmental Research Laboratories, National Severe Storms Laboratory, Norman, Oklahoma

28 October 1996 and 9 May 1997

ABSTRACT

Simulated WSR-88D (Weather Surveillance Radar-1988 Doppler) radar data were used to investigate the effects of discrete azimuthal sampling on Doppler velocity signatures of modeled mesocyclones and tornadoes at various ranges from the radar and for various random positions of the radar beam with respect to the vortices. Results show that the random position of the beam can change the magnitudes and locations of peak Doppler velocity values. The important implication presented in this study is that short-term variations in tornado and far-range mesocyclone intensity observed by a WSR-88D radar may be due to evolution or due to the chance positions of the radar beam relative to the vortex's maximum rotational velocities or due to some combination of both.

1. Introduction

A scanning Doppler radar's capability to measure thunderstorm mesocyclones and tornadoes is primarily dependent on the relationship between the vortex size and the size of a sample volume that the radar illuminates (which is a function of range from the radar, antenna beam size, and scan rate), as discussed by Donaldson (1970), Brown and Lemon (1976), Brown et al. (1978), Burgess and Lemon (1990), Burgess et al. (1993), and others. When a vortex's core diameter (distance between the peak rotational velocities) is significantly larger than the nominal diameter of the radar beam (distance between the half-power points), the vortex is well represented by Doppler velocity measurements. On the other hand, if the core diameter is smaller than the beam diameter, Doppler velocity values are degraded because of the smearing effects of the beam.

An additional problem that has not been considered in the literature is discrete azimuthal sampling that may or may not coincide with the peak rotational velocities in the vortex. It is not clear how radar sampling at discrete azimuthal intervals affects mean Doppler velocity measurements. Knowledge of the effects of discrete sampling is particularly important for addressing the problem of improving the Doppler radar detection of tornadoes and far-range mesocyclones.

Corresponding author address: Vincent T. Wood, NOAA/ERL/NSSL, 1313 Halley Circle, Norman, OK 73069.
E-mail: wood@nssl.noaa.gov

The objective of this paper is to investigate the effects of discrete sampling by a WSR-88D (Weather Surveillance Radar-1988 Doppler) radar on mesocyclone and tornadic vortex signatures. Though tailored specifically for WSR-88D operational parameters, the results shown are generally applicable to any Doppler radar. In section 2, a discussion is presented of the effects of discrete sampling on Doppler velocity signatures when a simulated WSR-88D-like radar scans across a Rankine (1901) combined vortex at various ranges from the radar and for various positions of the resolution volume with respect to the vortex. Section 3 discusses range variations of mean Doppler rotational velocities for Doppler velocity mesocyclone and tornado signatures. A concluding discussion is presented in section 4.

2. Effects of discrete sampling on Doppler velocity signatures

We developed an analytical model to investigate the effects of discrete sampling on Doppler velocity signatures of mesocyclones and tornadoes. The model used for the vortex was the Rankine combined vortex, where the rotational velocity increases linearly from zero at the center to a maximum at the core radius. Beyond the core radius, the rotational velocity decreases, with velocity being inversely proportional to distance from the rotation center. For simplicity, reflectivity is assumed to be uniform across the vortex. The simulation model generates Doppler velocity patterns that correspond to Rankine combined vortices located at various ranges from a Doppler radar. The model is similar to that developed by Zrnić and Doviak (1975) and used by Brown

and Lemon (1976) and Brown et al. (1978). The development and mathematical specifications of the model are given in appendix A.

For a rapidly scanning radar, the antenna can move a significant fraction of the angular beamwidth during the time it takes to collect the required number of samples to make an estimate of the mean Doppler velocity within a specific resolution volume. As a consequence, the circular beam is essentially broadened in the direction of antenna rotation, producing a larger *effective* horizontal beamwidth (i.e., Doviak and Zrnić 1993).

Presently, the WSR-88D can operate in two volume coverage patterns (VCPs) in precipitation mode. These VCPs are known as VCP 11, which scans 14 elevations in 5 min, and VCP 21, which scans 9 elevations in 6 min. On average, the WSR-88D's stationary beamwidth of 0.93° broadens to an effective horizontal beamwidth of approximately 1.29° for its precipitation mode of operation; see appendix B. The effective beamwidth is used for producing the simulated WSR-88D data presented in this paper.

a. Doppler velocity mesocyclone signatures

In this section, we investigate how the deduced mesocyclone strength and size are affected by the random position of the radar beam relative to the rotational velocity maxima in a mesocyclone. The model mesocyclone is axisymmetric with a Rankine combined velocity profile having a typical peak tangential velocity of 25 m s^{-1} at a core radius of 2.5 km. The velocity field was generated using Eq. (A.5) in appendix A. Figure 1 depicts simulated Doppler velocity patterns that correspond to the model mesocyclone. Each mean Doppler velocity value is represented by a uniformly colored range bin that extends 0.25 km in range and 1° in azimuth. The true mesocyclone center (black dot at the center of each dotted circle in the figure) was scanned by a radar located at 50, 100, 150, and 200 km from the mesocyclone center. When measured by the radar, a mesocyclone signature is identified as the visual pattern of azimuthally separated radial velocity maxima of opposite signs (''dark orange'' versus ''dark green''). In Fig. 1, each signature center is indicated by a white center point, and the white circle represents the ring of maximum measured rotational velocities. Doppler velocity patterns for angular separation values of −0.1°, −0.3°, and −0.5° (not shown) are mirror images of angular separations of +0.1°, +0.3°, and +0.5°. As illustrated in Fig. 2, angular separation is defined as the difference between the vortex center and the center of the nearest range bin. When data are collected at a discrete azimuthal sample interval of 1° (as used by the WSR-88D radar), the angular separation value of ±0.5°, for instance, between vortex center and range bin center means that the vortex center is positioned midway between two velocity range bins (between beams B and C in Fig. 1f and between beams A and B in Fig. 2a). A displacement of −0.3° from the vortex center (Fig. 2b) indicates that the nearest range bin center C is positioned 0.3° to the left of the vortex center. The angular separation varies between ±0.5°, which represents the full azimuthal sample interval.

Figure 1 compares the appearances of the Doppler velocity patterns at a close range (where the core diameter was considerably larger than the range-dependent beam diameter) with those at more distant ranges (where the beam diameter approached the core diameter). Doppler velocities are degraded owing to the widening of the beam with range relative to the vortex size, as reflected in the ratios of beam diameter to core diameter given along the right side of the figure.

When the range bin is nearly centered on the mesocyclone at long ranges (e.g., Fig. 1a), the Doppler velocity patterns show a clear separation between peak Doppler velocities with a band of near-zero velocities running through the mesocyclone signature center. With increasing angular separation between the true mesocyclone center and range bin center, the Doppler velocity peaks occur at adjacent range bins (e.g., Fig. 1c). Consequently, deduced core diameters (white lines connecting the measured peak Doppler velocity values) decrease.

Why does the pattern of the mesocyclone signature fluctuate as the angular separation changes from +0.1° to +0.5° in Fig. 1? To help understand this question, we refer to Fig. 3, which shows the azimuthal profile (normal to the radar viewing direction) of Doppler velocity values (black dots) through a mesocyclone at 150-km range (Figs. 3d–f correspond to Figs. 1d–f). When the angular separation is +0.1° at this particular range (Fig. 3d), data points B and D essentially coincide with the locations of the negative and positive velocity peaks, producing a mean rotational velocity of 18.2 m s^{-1}. Positions B and D are separated by two azimuthal increments. Figure 1d indicates that the deduced (white) and true (black dotted) core regions are essentially identical (5.2- versus 5.0-km core diameters). When the radar samples the mesocyclone with an angular separation of +0.3° (Figs. 1e and 3e), the core region remains the same size because the extreme measured velocities (B and D) are still separated by two azimuthal increments. However, the mean rotational velocity has decreased to 16.7 m s^{-1} because B and D are no longer at the peaks of the measured curve. When the mesocyclone is centered midway between two range bins (angular separation of ±0.5°, Figs. 1f and 3f), the extreme measured values (A and D) are separated by three azimuthal increments, and so the deduced diameter has increased to 7.9 km and the mean rotational velocity has decreased slightly to 16.4 m s^{-1}.

Variations in mesocyclone signatures that contribute to a constantly changing appearance between volumetric scans could be interpreted as mesocyclone evolution. However, it is important to recognize that variations also are caused by different positions of the beam center relative to the mesocyclone's rotational velocity maxima. Variations related to radar sampling affect the ap-

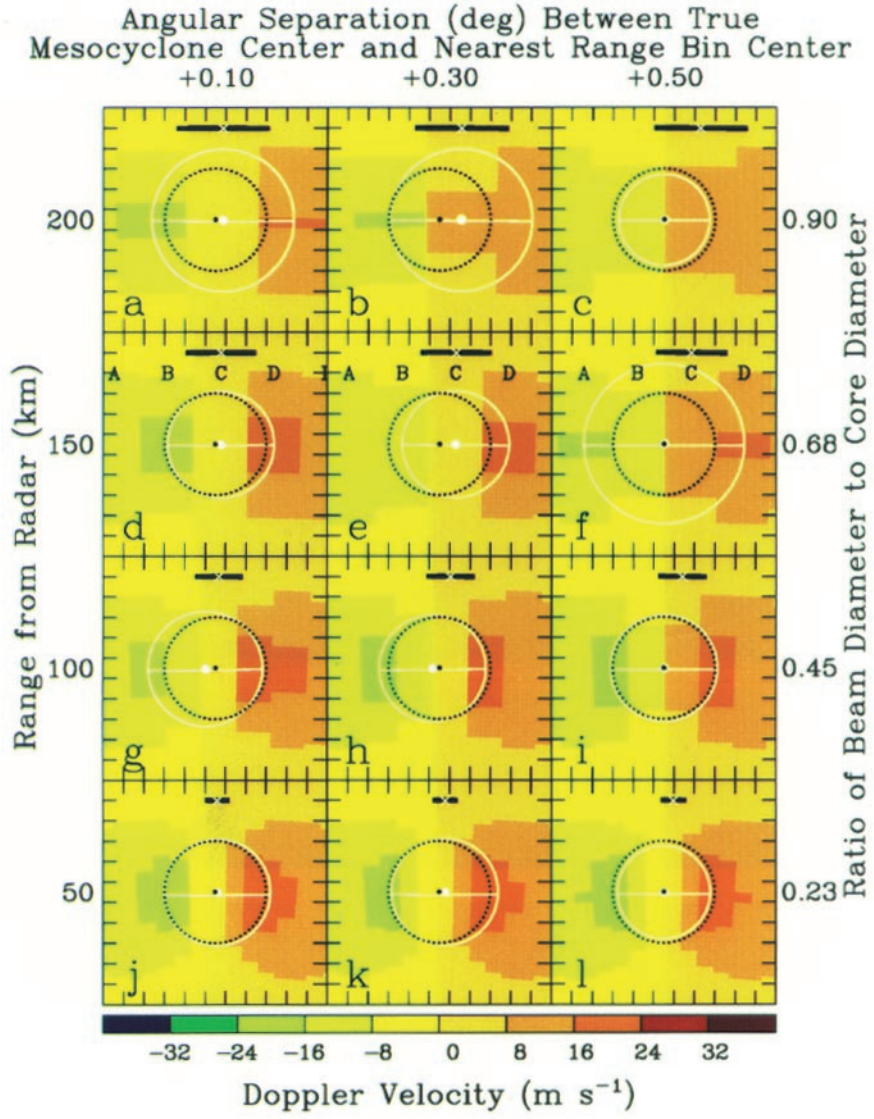

FIG. 1. Plan views of simulated Doppler velocity mesocyclone signatures measured by a radar located 50, 100, 150, and 200 km from a Rankine combined vortex center. Negative (positive) Doppler velocities to the left (right) of the vortex center represent flow toward (away from) the radar. Each dotted black circle, around its black center point, represents the true circle of maximum wind speed (25 m s^{-1} at radius of 2.5 km) for the model mesocyclone. Each white circle, around its white signature center point, represents the deduced size of the core region based on the peak Doppler velocity measurements. The black bar represents the radar resolution volume size broadened by antenna motion (effective beamwidth of 1.29°) for beam C; a white X represents the center of the resolution volume. Beams A, B, C, and D are identified in (d)–(f). Border tick marks are 1 km apart. Data resolution is 1° azimuth by 0.25-km range. Angular separation (°) between the true mesocyclone center and beam center is shown at the top. The ratio of radar beam diameter to core diameter is shown on the right. The radar is located beyond the bottom of the figure.

pearance of mesocyclone signatures and make proper interpretation of temporal and spatial variations difficult.

b. Doppler velocity tornado signatures

Brown et al. (1978) discussed important characteristics of the tornadic vortex signature (TVS), which occurs when the diameter of the radar beam is larger than the tornado vortex. A TVS is a Doppler velocity signature of large shear, coincident with the tornado-scale circulation, characterized by Doppler velocity maxima of opposite signs occurring approximately one beamwidth apart. Not all tornadoes produce identifiable signatures because TVS detection is a function of tornado

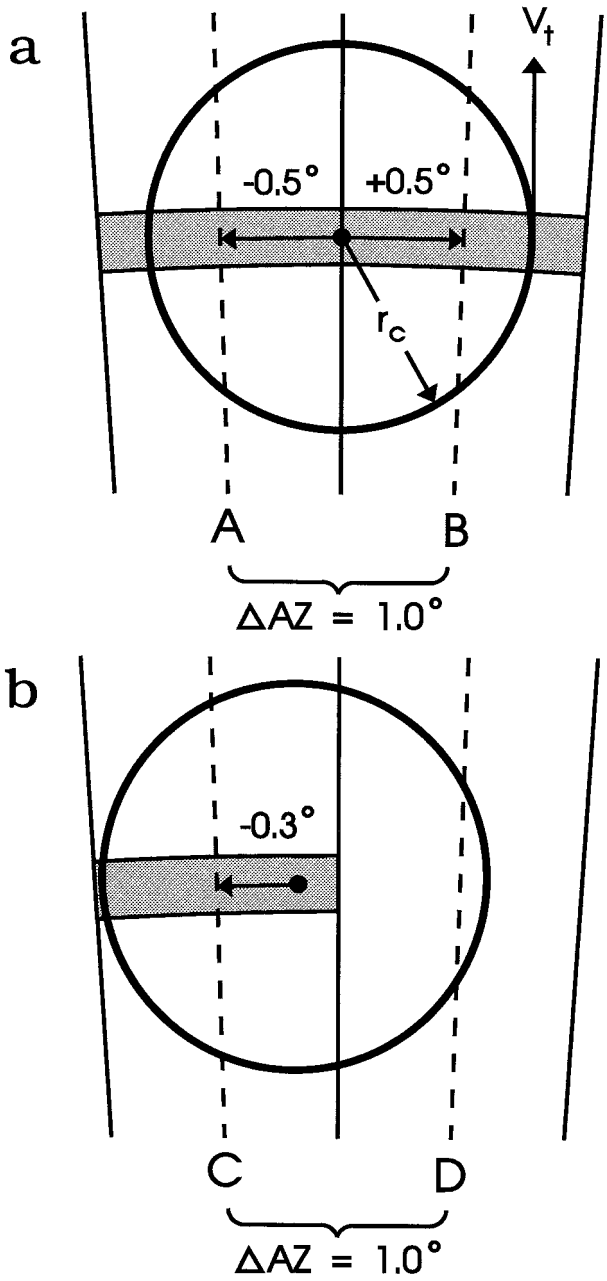

FIG. 2. Relationship of the center (dashed radial) of the radar's resolution volume to the true vortex center (black dot). A shaded band represents a range bin that extends 0.25 km wide in range and 1° wide in azimuth. The letters A, B, C, and D indicate the centers of the resolution volumes; the discrete azimuthal sample interval (ΔAZ) between range bin centers is 1°. The solid radial lines represent the azimuthal limits of each displayed Doppler velocity value like those in Figs. 1 and 4. The circle represents the vortex's ring of maximum tangential velocity (V_t) at its core radius (r_c). The radar is located beyond the bottom of the figure. In (a) the vortex center is equidistant between the centers of two range bins, whereas in (b) the center of the nearest range bin is 0.3° to the left of the vortex center.

core diameter and strength as well as the size of the radar sampling volume.

Because all but the largest and closest tornadoes have diameters that are smaller than the radar beam, the tornado's rotational velocities are greatly smoothed owing to Gaussian-weighted averaging within the radar beam (e.g., Brown and Lemon 1976; Burgess and Lemon 1990). Because of the smearing effects of a large radar beam on a small tornado vortex, the deduced azimuthal diameter of the TVS always overestimates the core diameter of the tornado, and the peak rotational velocity of the TVS always underestimates the peak rotational velocity of the tornado. Thus, Doppler velocities within the resulting TVS do not reflect either the size or strength of the tornado but rather some indeterminable combinations of the two parameters (e.g., Brown et al. 1978). (This discussion also applies to small mesocyclones at great range from the radar.)

A hypothetical F4 (Fujita 1981) tornado (assuming a Rankine combined vortex) having a peak tangential velocity of 100 m s^{-1} at a core radius of 0.25 km is used to illustrate the effects of the radar's beamwidth on TVSs. Although strong tornadoes occur within mesocyclones, a model mesocyclone was not included in this simulation in order to emphasize TVS characteristics. Figure 4 presents Doppler velocity data with 1° azimuthal and 0.25-km range resolution (same as in Fig. 1). The Doppler velocity patterns correspond to a tornado located 5, 50, 100, and 150 km from the radar.

The Doppler velocity patterns centered at 5-km range in Figs. 4j–l do not represent a TVS, but rather represent the tornado itself because the tornado is much larger than the diameter of the beamwidth at this close range. At this range, the deduced core diameter is close to the true core diameter and the deduced rotational velocities are 85%–90% of the true value. Here, variations in the angular separation do not produce significant differences in the single-Doppler velocity pattern. However, the overall pattern is distorted owing to proximity to the radar (e.g., Wood and Brown 1992).

Variations in TVS related to radar sampling significantly affect the appearance of Doppler velocity TVS patterns at greater ranges from the radar (Fig. 4). The reason that TVS peak velocities are separated by two azimuthal sampling intervals for near-zero (+0.1°) separation angles and by one azimuthal sampling interval at greater (+0.3°, +0.5°) separation angles is illustrated in Fig. 5. Figures 5d–f at 50-km range correspond to Figs. 4g–i. When a beam is essentially centered on the tornado (C in Fig. 5d), the peak negative and positive velocity data points (B and D) are always separated by two azimuthal sampling intervals. The Doppler velocity pattern in Fig. 4g could be interpreted as that of a small but strong mesocyclone, although the pattern represents the TVS. At the other extreme, when the tornado is centered midway between two range bins (Fig. 5f), the peak velocity data points (B and C) are adjacent to each other and therefore produce a stronger tornadic vortex

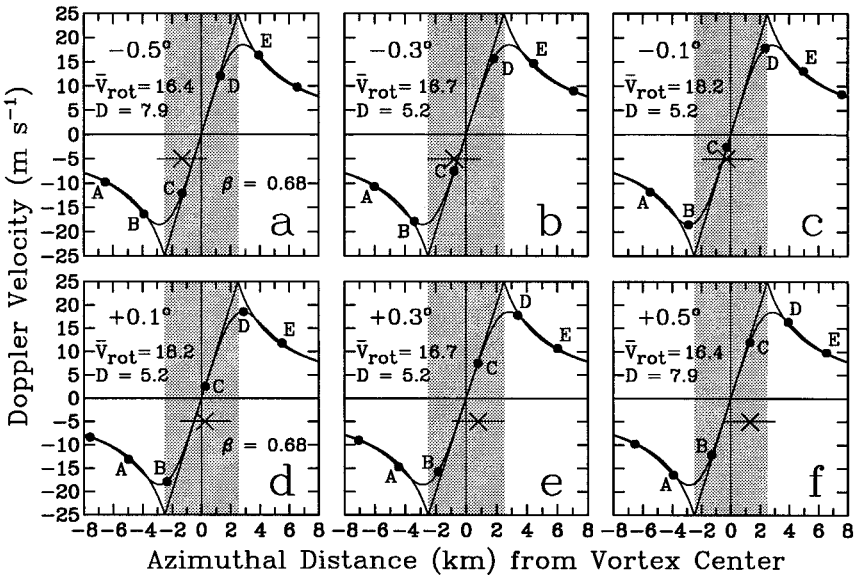

FIG. 3. Relationships of data points relative to the azimuthal profiles of a mesocyclone as a function of angular separation values. Continuous and discrete samplings of Doppler velocity azimuthal profiles across the center of a mesocyclone at 150-km range are indicated, respectively, by the solid nonpointed curve and superimposed dots, for a ratio (β) of beam diameter to core diameter of 0.68. The true azimuthal profile of the mesocyclone is indicated by the curve with pointed peaks. Vertical shading represents the 5-km core region of the model vortex having a peak tangential velocity of 25 m s^{-1}. Negative (positive) Doppler velocities (m s^{-1}) to the left (right) of the mesocyclone axis represent flow toward (away from) the radar. The data points at A, B, C, D, and E represent successive positions of the radar beam center at 1° azimuthal increments as the beam scans across the mesocyclone. Just below the zero Doppler velocity line, the horizontal line centered on X represents the effective half-power beamwidth (nominal resolution volume) that indicates the location of beam C (also shown in Fig. 1). Angular separation values of −0.5°, −0.3°, −0.1°, +0.1°, +0.3°, and +0.5° between the mesocyclone center and the closest beam center are indicated. Mean rotational velocity (m s^{-1}) is calculated from $\overline{V}_{rot} = 0.5(V_{max} - V_{min})$; D is the deduced core diameter (km) between V_{min} and V_{max}. (d)–(f) As in Figs. 1d–f.

signature (Fig. 4i). It therefore is important to recognize that the random position of the beam center relative to the tornado's rotational velocity maxima can change the magnitudes and locations of mean Doppler velocity peaks.

3. Range variation of the mean Doppler rotational velocities

In the examples shown thus far, mean rotational velocities have been computed for only a few angular separations at a few ranges from the radar. Figures 6 (mesocyclone) and 7 (tornado) show the effect of radar sampling on the mean rotational velocity $\overline{V}_{rot}$ for all ranges from 10 to 230 km; $\overline{V}_{rot} = 0.5(V_{max} - V_{min})$. In these figures, the vertical width of the shaded bands represents the full spread of $\overline{V}_{rot}$ values computed for 51 angular separation values between −0.5° and +0.5°, while the thick line running down the middle of each band is the mean of the 51 $\overline{V}_{rot}$ values at each range. The vertical width varies in a systematic manner with increasing range owing to the increasing azimuthal separation of data points and their varying positions relative to the peaks of the measured Doppler velocity profiles. Each time the width narrows with increasing range, the number of azimuthal intervals between the Doppler velocity peaks decreases by one. When the ratio of beam diameter to core diameter is greater than 1–2 (beyond 25–40 km in Figs. 4 and 7), the vertical width of the shaded bands becomes more uniform because the number of azimuthal intervals between the measured Doppler velocity peaks no longer decreases but remains constant at one or two (as shown in Fig. 5).

To present a basic understanding of the effects of discrete azimuthal sampling on mesocyclone and tornadic vortex signatures, we have used noise-free simulated data up to this point. In reality, WSR-88D Doppler velocity measurements include errors that have a standard deviation of about 1.0 m s^{-1}. In our simulations, this uncertainty was included by adding Gaussian-distributed random noise (see appendix A) to each Doppler velocity value. After the addition of noise to data points, such as those in Figs. 3 and 5, they no longer lie on the corresponding theoretical curves. The mean rotational velocity $\overline{V}_{rot}$ is different, and the di-

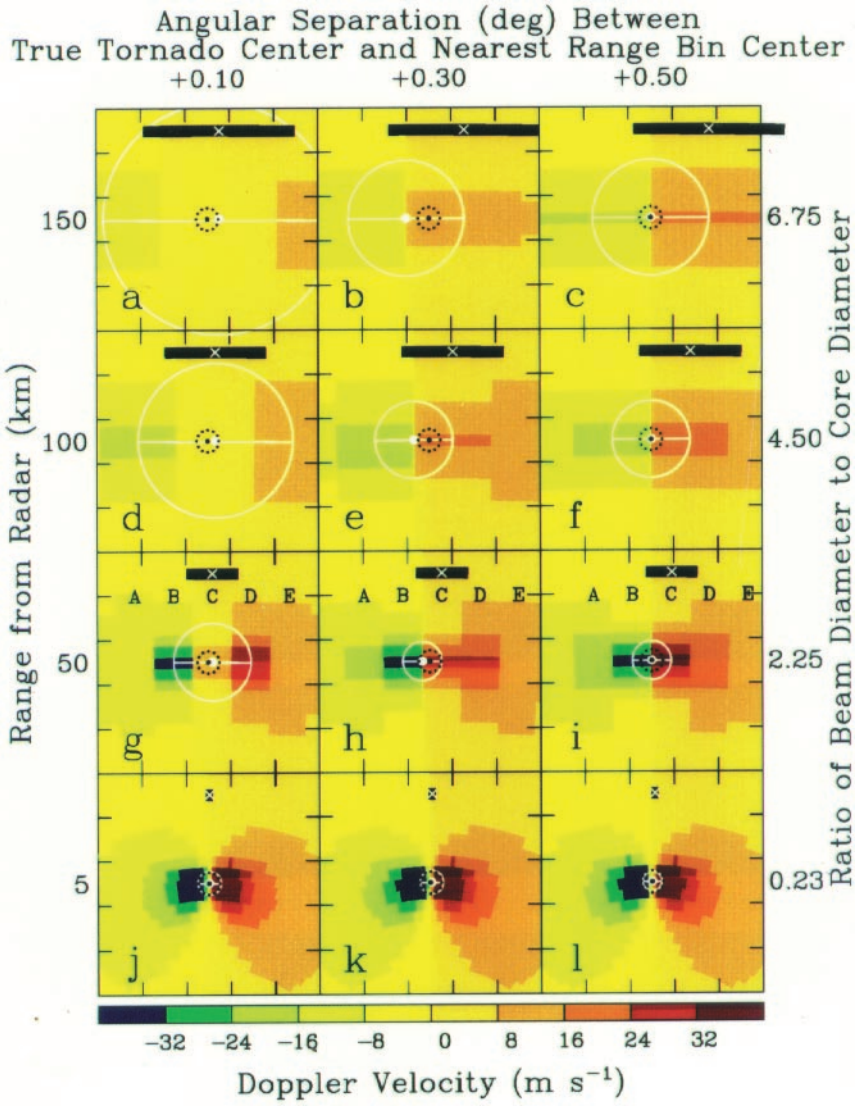

FIG. 4. Same as Fig. 1 except that this is the plan view of a simulated Doppler velocity TVS for a radar located 5, 50, 100, and 150 km from a Rankine combined vortex center. The maximum wind speed is 100 m s^{-1} and is located at 0.25 km from the model tornado center.

ameter will change if the new peak value jumps to an adjacent data point.

Figures 8 and 9 show how the spread of estimated rotational velocities in mesocyclone and tornadic vortex signatures increases with the inclusion of Gaussian-distributed random noise. For mesocyclones at close range, a given $\overline{V}_{rot}$ value can lie anywhere over an interval of about 3 m s^{-1} due to the random position of beam center relative to mesocyclone center. The interval increases to about 5 m s^{-1} at far ranges of 150 km or more. For a TVS associated with an F4 tornado at close range, the interval over which $\overline{V}_{rot}$ would randomly occur is more than 10 m s^{-1}. The interval gradually narrows to 6–7 m s^{-1} at ranges of more than 200 km.

4. Concluding discussion

It is widely recognized that Doppler radar suffers from a resolution-related problem in observing Doppler velocity signatures of mesocyclones and tornadoes. The problem arises from the degradation of Doppler velocities owing to the widening of the radar beam with range relative to the vortex size, as discussed by Donaldson (1970), Brown and Lemon (1976), Brown et al. (1978), Burgess and Lemon (1990), Burgess et al. (1993), and others. The current study extends the discussion of resolution-related problems to include radar sampling at discrete azimuth intervals, which can significantly affect the magnitudes and locations of Doppler velocity peaks associated with vortices.

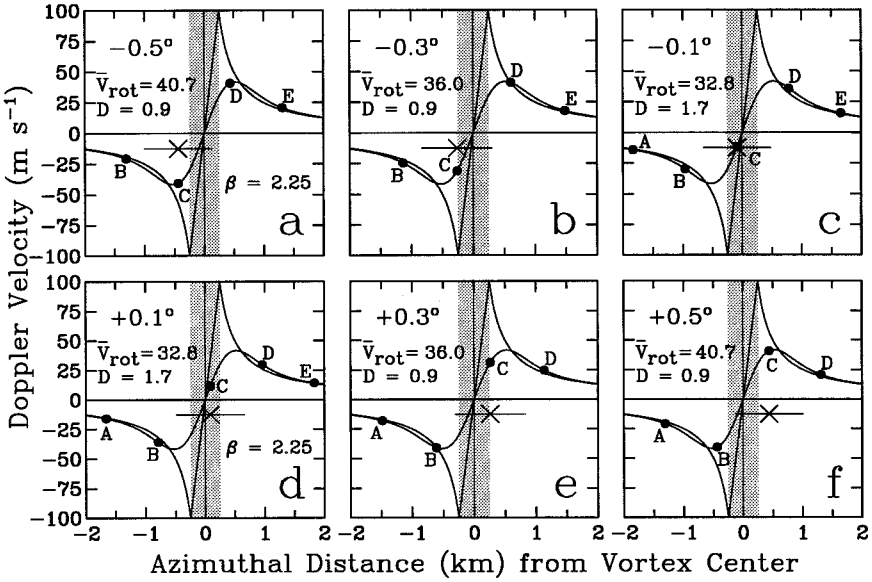

FIG. 5. Same as Fig. 3 except for a tornado at 50-km range and a beam diameter to core diameter ratio of 2.25; the model vortex has a peak tangential velocity of 100 m s^{-1} at a radius of 0.25 km. (d)–(f) As in Figs. 4g–i.

We studied the effects of radar sampling on single-Doppler velocity signatures of thunderstorm mesocyclones and tornadoes by simulating a WSR-88D radar scanning across Rankine combined vortices at various ranges from the radar and for various azimuthal separation distances between range bin centers and vortex centers. Results reveal that with WSR-88D data collected in a discrete manner, the random positions of the radar beam relative to the mesocyclone or tornado center modify the magnitudes and azimuthal separations of the Doppler velocity peaks. Such magnitudes and locations depend heavily on how close the beam center is to the vortex's maximum rotational velocities at either edge of the vortex core. As a consequence, variations in single-Doppler velocity signatures of mesocyclones and tornadoes can contribute to constantly changing appearances that could be misinterpreted as changes in mesocyclone or tornado intensity.

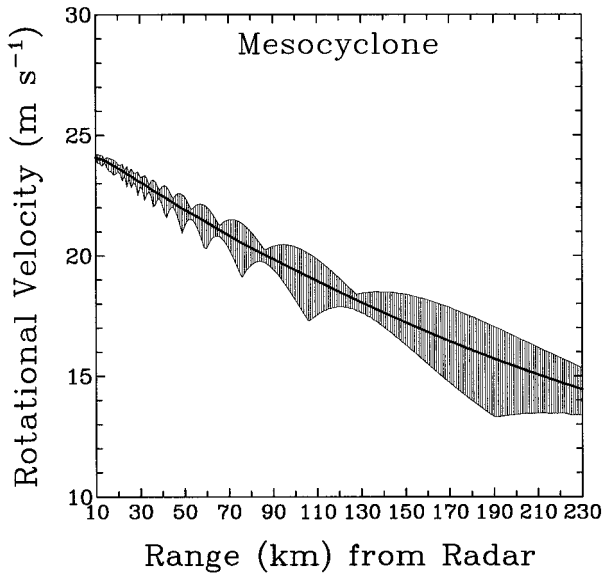

FIG. 6. Variations of $\bar{V}_{rot}$ for average-sized mesocyclone signatures as a function of range. Shading represents the full spread of $\bar{V}_{rot}$ values for all angular separations between range bin centers and vortex centers, and the heavy curve represents the mean of the $\bar{V}_{rot}$ values at each range.

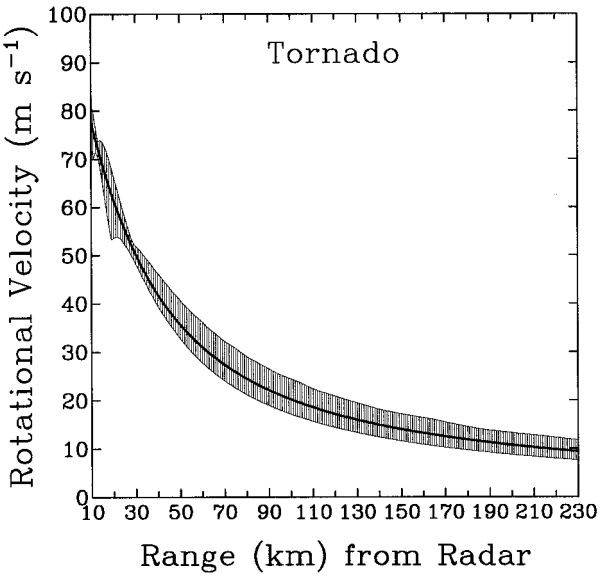

FIG. 7. Same as Fig. 6 except for Doppler velocity tornadic vortex signature associated with an F4 tornado.

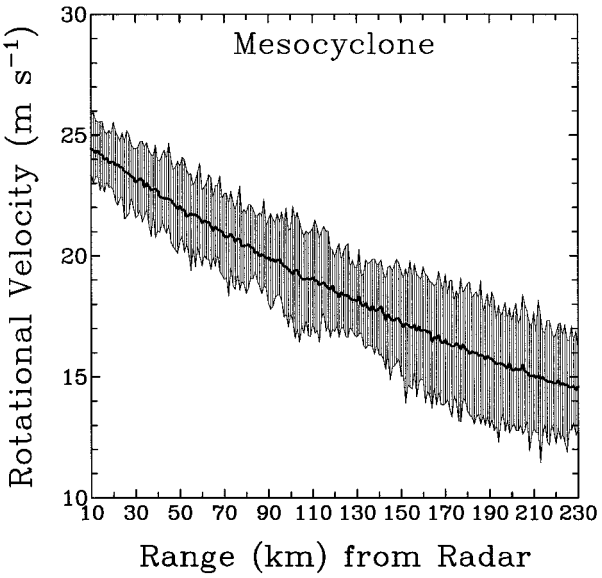

FIG. 8. Same as Fig. 6 except that Gaussian-distributed random noise was added to the individual Doppler velocity data points used to compute the mean rotational velocity.

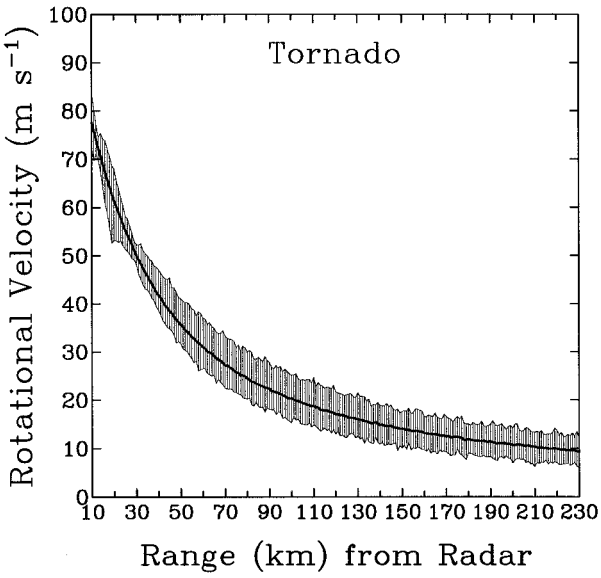

FIG. 9. Same as Fig. 7 except that Gaussian-distributed random noise was added to the individual Doppler velocity data points used to compute the mean rotational velocity.

An important implication presented in this study is that short-term variations in tornado and far-range mesocyclone intensity observed by a WSR-88D radar (or any Doppler radar) may be due to evolution or due to the chance positions of the radar beam relative to the vortex's maximum rotational velocities or due to some combination of both. It is not possible to determine which one produces these variations. Therefore, it is very important to recognize that data interpretation is affected by discrete azimuthal sampling. For instance, if a time–height plot of the Doppler mesocyclone rotational velocity or velocity difference across the TVS is prepared, the values may appear to be rather noisy, owing to the fact that the peak values in the resulting signature may or may not be the actual peak values in the mesocyclone or TVS. Vasiloff (1993) and Trapp and Mitchell (1995), for example, discussed TVS evolution based on time–height plots of single-Doppler radar data. Careful inspection of these data reveal smaller-scale closed contours of TVS velocity differences that might be an artifice of radar sampling. Another example is that of the Wakimoto and Martner (1992) case study. They combined high-resolution single-Doppler radar measurements with photographs to reveal the detailed structural relationship of a tornado's reflectivity and Doppler velocity fields with its visual features seen in proximity to the National Oceanic and Atmospheric Administration's Wave Propagation Laboratory (now Environmental Technology Laboratory) 3-cm radar. Careful examination of the Doppler velocity data reveals that there are several pockets of Doppler velocity maxima on either side of the tilted tornado at different times; they could be a consequence of radar sampling.

In this preliminary study of the effects of discrete azimuthal sampling on single-Doppler velocity signatures of mesocyclones and tornadoes, we have used 1) two-dimensional horizontal sampling [e.g., see Eq. (A.4)], 2) a uniform reflectivity field in which the vortices are embedded, and 3) constant vertical profiles of rotating velocities in the vortex region. In future studies, we will include three-dimensional sampling, variable reflectivity fields, and nonuniform vertical profiles of vortex rotation.

Acknowledgments. The authors thank Dusan Zrnić, Richard Doviak, Erik Rasmussen, and Mike Eilts, all of NSSL, and Dale Sirmans, of WSR-88D Operational Support Facility (OSF), for their helpful reviews at various stages in the preparation of the manuscript. Appreciation is expressed to Kurt Hondl and Bob Davies-Jones, of NSSL; Leslie Torok of Data Acquisition Systems Branch of Environment Canada in Downsview, Ontario, Canada; and Allen Zahrai of WSR-88D OSF; for their helpful comments. The authors thank Steve Smith, Mike Istok, and Dan Purcell of WSR-88D OSF for providing us the WSR-88D radar data acquisition parameters shown in Table B.1. The suggestions by two anonymous reviewers have contributed to the improvement of the manuscript.

APPENDIX A

Description of a Simulation Model

We briefly describe an analytical model that generates Doppler velocities corresponding to the component of a three-dimensional wind vector as a function of azimuth, range, and elevation from a Doppler radar. The

mean Doppler velocity $\overline{v}_d(\theta_0, r_0, \phi_0)$ at the center range r_0, azimuth angle θ_0, and elevation angle ϕ_0 of the effective resolution volume of the radar beam in the simulations (Doviak and Zrnić 1993) may be written in a general form:

$$\overline{v}_d(\theta_0, r_0, \phi_0) = \frac{\sum_{i=1}^{I}\sum_{j=1}^{J}\sum_{k=1}^{K} v_d(\theta, r, \phi)|W(r)|^2 f^4(\theta, \phi)\eta(\theta, r, \phi)}{\sum_{i=1}^{I}\sum_{j=1}^{J}\sum_{k=1}^{K} |W(r)|^2 f^4(\theta, \phi)\eta(\theta, r, \phi)}, \quad \text{(A.1)}$$

where I, J, and K are, respectively, an odd number of subpoints in azimuth θ_i, range r_j, and elevation ϕ_k centered on the effective resolution volume; $v_d(\theta, r, \phi)$ and $\eta(\theta, r, \phi)$ are, respectively, the Doppler velocity component and radar reflectivity values at each subpoint; $|W(r)|^2$ is the magnitude of the two-way range weighting function with a 6-dB width r_6 of the resolution volume in range; and $f^4(\theta, \phi)$ is the two-way antenna pattern weighting function.

The range weighting function $|W(r)|^2$ in Eq. (A.1) is used to weight the Doppler velocity values at the r_j data point and may be calculated from

$$|W(r)|^2 = \left(1 - \left|\frac{r_j - r_0}{r_6}\right|\right)^2, \quad \text{(A.2)}$$

where $r_6 = 235$ m for the usual WSR-88D mode of operation. In an analogous way, the antenna pattern weighting function $f^4(\theta, \phi)$ in Eq. (A.1) is used to weight the Doppler velocity values at the θ_i, ϕ_k data point and is given by

$$f^4(\theta, \phi) = \exp\left\{-4\ln 4\left[\left(\frac{\theta_i - \theta_0}{\theta_e}\right)^2 + \left(\frac{\phi_k - \phi_0}{\phi_1}\right)^2\right]\right\}, \quad \text{(A.3)}$$

where θ_e is the one-way effective horizontal beamwidth (discussed in appendix B) and ϕ_1 is the one-way vertical beamwidth. Equation (A.3) is a simple Gaussian function that neglects the effects of antenna sidelobes.

In this study, we treat a simplified two-dimensional problem (horizontal x–y plane) and make the following assumptions: 1) the velocity field is uniform with height, 2) reflectivity is uniform, and 3) the beam axis is horizontal. In our preliminary experiments, we calculated $\overline{v}_d(\theta_0, r_0, \phi_0)$ using Eq. (A.1) and compared it with that produced by two-dimensional sampling. We found that the results were essentially identical because the velocity field was constant with height. A uniform reflectivity field was selected for this study because we wanted to present the basic aspects of the discrete radar sampling problem without the added interpretation complications introduced by nonuniform reflectivity patterns; a variety of nonlinear reflectivity profiles will be investigated in a follow-on study. For these reasons and for increased computational efficiency, we reduced Eq. (A.1) to the two-dimensional problem, as given by

$$\overline{v}_d(\theta_0, r_0) = \frac{\sum_{i=1}^{I}\sum_{j=1}^{J} v_d(\theta, r)|W(r)|^2 f^4(\theta)}{\sum_{i=1}^{I}\sum_{j=1}^{J} |W(r)|^2 f^4(\theta)}, \quad \text{(A.4)}$$

where $I = 21$ and $J = 5$ for these simulations. The horizontal cross section of the nominal resolution volume associated with Eq. (A.4) is shown in Fig. A1. The mean simulated Doppler velocity $\overline{v}_d(\theta_0, r_0)$ is averaged over the nominal width equal to twice the effective horizontal beamwidth in order to produce a more representative value. Tests indicated that the range weighting function did not have to be extended beyond the range width r_6 shown in Fig. A1.

In Eq. (A.4), the Doppler velocity component v_d at range r is the component of the wind vector in the azimuth direction θ from the radar. As derived by Wood and Brown (1992), the Doppler velocity value is calculated explicitly from the Rankine velocity field at each subpoint i, j of the $I \times J$ matrix within the beam is given by

$$v_d(\theta, r) = V_t\left(\frac{r_d}{r_c}\right)^{\lambda}\frac{R_c}{r_d}\sin(\theta_i - \theta_c), \quad \text{(A.5)}$$

where V_t is the peak tangential velocity at the core radius r_c, $r_d = [R_c^2 + r_j^2 - 2R_c r_j \cos(\theta_i - \theta_c)]^{1/2}$ is the distance from the vortex center to the subpoint, and the exponent λ describes the radial profile of the tangential wind component ($\lambda = 1$ for $r_d \le r_c$ and $\lambda = -1$ for $r_d > r_c$). Here, R_c and θ_c represent the center range and azimuth, respectively, of the vortex from the radar. In the Rankine combined vortex, tangential velocity increases linearly from the circulation center, where velocity is zero, to the core radius where the tangential velocity attains its maximum value. Beyond the core radius, the tangential velocity decreases in a manner inversely proportional to distance from the circulation center.

To produce mean Doppler velocity values that are closer to reality, one can add Gaussian-distributed random noise (RG) to the velocity values:

$$\overline{v}'_d(\theta_0, r_0) = \overline{v}_d(\theta_0, r_0) + RG, \quad \text{(A.6)}$$

where

$$RG = \left(\sum_{n=1}^{N} RW_n - 0.5N\right)\sigma_G(N/12)^{-1/2}$$

is Gaussian-distributed random noise having a mean value of zero and standard deviation of σ_G. Here, RW is a random number from a white noise generator where the random values are evenly distributed between 0.0 and 1.0. A value of $N = 30$ was chosen for the noisy data shown in Figs. 8 and 9.

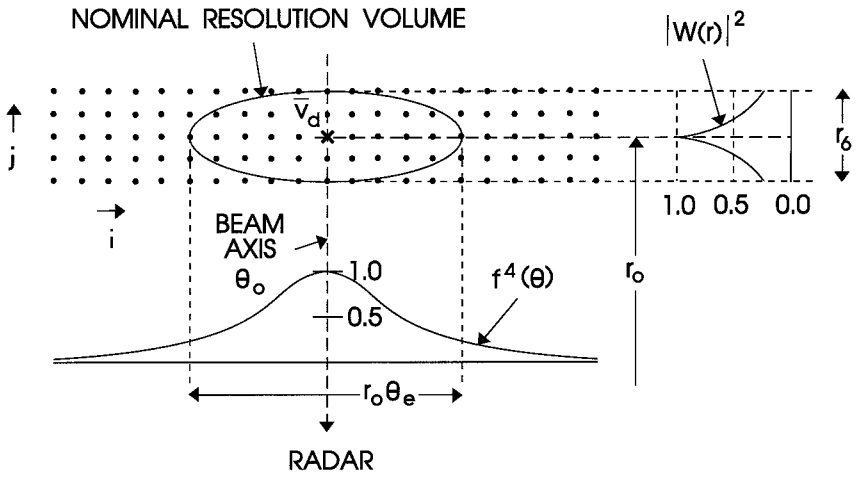

FIG. A1. Horizontal cross section of a nominal radar resolution volume associated with Eq. (A.4); $f^4(\theta)$ is the two-way antenna pattern weighting function; $|W(r)|^2$ is the range weighting function with associated 6-dB range width r_6; θ_e is the one-way effective horizontal beamwidth. The *i, j* subpoints are indicated by dots. The center range r_0 and azimuth θ_0 the mean Doppler velocity value $\overline{v}_d$ is indicated by an ×. (After Doviak and Zrnić 1993.)

APPENDIX B

Calculation of Effective Beamwidth

The horizontal beamwidth is effectively broadened when the antenna moves a significant amount while transmitting the pulses required to compute a representative Doppler velocity value. For our simulations, we determine the effective horizontal beamwidth based on typical values for the WSR-88D radar data acquisition parameters (α, M, T_s, θ_1); this approach can be applied to any radar. Expressed by Doviak and Zrnić (1993), the effective beamwidth θ_e is a function of antenna rotation rate α, number M of pulses sampled to compute the mean Doppler velocity value, pulse repetition period T_s (inversely proportional to pulse repetition frequency), and one-way beamwidth θ_1 between half-power points. The effective beamwidth may be computed from

$$\text{erf}[2(\ln 4)^{1/2}\theta/\theta_1] - \text{erf}[2(\ln 4)^{1/2}(\theta - \alpha M T_s)/\theta_1] - 0.5\ \text{erf}[(\ln 4)^{1/2}\alpha M T_s/\theta_1] = 0, \quad \text{(B.1)}$$

where the error function erf(x) is defined by

$$\text{erf}(x) = 2\pi^{-1/2}\int_0^x \exp(-\xi^2)\, d\xi. \quad \text{(B.2)}$$

Equation (B.1) has two solutions θ_a and θ_b that determine the effective beamwidth $\theta_e = \theta_b - \theta_a$. To obtain the solutions, one applies an iteration method to (B.1) by using $\theta_{i+1} = \theta_i + \delta\theta$, where $\delta\theta$ is a very small value of azimuthal interval (say, 0.001°) and guessing the first value of θ_a (say, 0.1°). Equation (B.1) is iterated until it sufficiently converges toward zero. Then, the resulting θ_{i+1} is set to θ_b. Similarly, the iteration method is applied to θ_a, except that θ_i and $\delta\theta$ are initially negative values.

Table B1 gives representative values of V_N, α, M, T_s, and θ_e for a typical WSR-88D radar. In addition to the representative values, the table gives the range of values (NWS 1992). The beamwidths for WSR-88D radars range from 0.88° to 0.97°, and the corresponding wavelengths range from 10.0 to 11.1 cm. The overall mean values of beamwidth and wavelength are, respectively, 0.93° and 10.6 cm; these values are used in this study.

The WSR-88D's VCPs specify the actual elevation

TABLE B1. For data collection using volume coverage patterns (VCPs) 11 and 21, representative values of Nyquist velocity V_N, antenna rotation rate α, number of pulses sampled M, and pulse repetition period T_s were used to calculate effective horizontal beamwidth θ_e for four different WSR-88D volume scan strategies (NWS 1992). The values in parentheses indicate the variation among individual WSR-88D radars or the variation within a given VCP from one elevation angle to the next. The average one-way beamwidth for WSR-88D radars is 0.93°.

VCP	V_N (m s^{-1})	α (° s^{-1})	M (No. of pulses)	T_s (ms)	θ_e (°)
11	25	18 (16.1–19.2)	44 (41–52)	1.06	1.272 (1.174–1.461)
11	32	18 (16.1–19.2)	55 (50–66)	0.83	1.257 (1.151–1.453)
21	25	11 (11.2–11.4)	76 (70–88)	1.06	1.329 (1.268–1.461)
21	32	11 (11.2–11.4)	96 (88–111)	0.83	1.319 (1.257–1.448)
				Mean	1.29

TABLE B2. Comparison of beam diameters at various ranges for beamwidths of 0.93° and 1.29°.

Range (km)	Beam diameter (km)	
	$\theta_1 = 0.93°$	$\theta_e = 1.29°$
50	0.81	1.13
100	1.62	2.25
150	2.43	3.38
200	3.25	4.50
230	3.73	5.18

angles at which the antenna is positioned during a volume scan. The antenna rotation rate, number of pulses sampled, and pulse repetition period vary as a function of elevation angle. In Table B1, VCP 11 and 21 are chosen because these data collection modes are used in severe thunderstorm situations. The mean values of the antenna rotation rate α and the number of pulses sampled M are representative of elevation angles below 7°, which encompass the depth of typical mesocyclones and tornadoes at most ranges of interest. With the overall mean WSR-88D's wavelength of 10.6 cm, the typical values of pulse repetition periods T_s are based on the typical Nyquist velocities V_N of 25 and 32 m s^{-1}. Therefore, an overall mean value of effective beamwidth θ_e is obtained by averaging four individual effective beamwidths, which are calculated from Eq. (B.1). Consequently, the overall mean effective beamwidth for the two VCPs and for two Nyquist velocities is 1.29° for the simulations discussed in this paper.

Table B2 compares beam diameter as a function of range for the mean beamwidth of a stationary antenna (0.93°) and the mean effective beamwidth of a rapidly scanningly antenna (1.29°). Diameter of the 1.29° effective beamwidth is approximately 1.4 as wide as that of the 0.93° stationary beamwidth.

REFERENCES

Brown, R. A., and L. R. Lemon, 1976: Single Doppler radar vortex recognition. Part II: Tornadic vortex signatures. Preprints, *17th Conf. on Radar Meteorology*, Seattle, WA, Amer. Meteor. Soc., 104–109.

——, ——, and D. W. Burgess, 1978: Tornado detection by pulsed Doppler radar. *Mon. Wea. Rev.*, **106,** 29–38.

Burgess, D. W., and L. R. Lemon, 1990: Severe thunderstorm detection by radar. *Radar in Meteorology*, D. Atlas, Ed., Amer. Meteor. Soc., 619–656.

——, R. J. Donaldson Jr., and P. R. Desrochers, 1993: Tornado detection and warning by radar. *The Tornado: Its Structure, Dynamics, Prediction, and Hazards, Geophys. Monogr.*, No. 79, Amer. Geophys. Union, 203–221.

Donaldson, R. J., Jr., 1970: Vortex signature recognition by a Doppler radar. *J. Appl. Meteor.*, **9,** 661–670.

Doviak, R. J., and D. S. Zrnić, 1993: *Doppler Radar and Weather Observations.* Academic Press, 562 pp.

Fujita, T. T., 1981: Tornadoes and downbursts in the context of generalized planetary scales. *J. Atmos. Sci.*, **38,** 1511–1534.

NWS, 1992: Operation instructions Unit Control Position (UCP), Doppler meteorological radar WSR-88D. Manual NWS EHB 6-521, 1-58–1-60, 9-44, 9-45, 577 pp. [Available from NOAA Logistics Supply Center, Kansas City, MO 64131.]

Rankine, W. J. M., 1901: *A Manual of Applied Mechanics.* 16th ed. Charles Griff and Company, 680 pp.

Trapp, R. J., and E. D. Mitchell, 1995: Characteristics of tornadic vortex signatures detected by WSR-88D radars. Preprints, *27th Conf. on Radar Meteorology*, Vail, CO, Amer. Meteor. Soc., 211–212.

Vasiloff, S. V., 1993: Single-Doppler radar study of a variety of tornado types. *The Tornado: Its Structure, Dynamics, Prediction, and Hazards, Geophys. Monogr.*, No. 79, Amer. Geophys. Union, 223–232.

Wakimoto, R. M., and B. E. Martner, 1992: Observations of a Colorado tornado. Part II: Combined photogrammetric and Doppler radar analysis. *Mon. Wea. Rev.*, **120,** 522–543.

Wood, V. T., and R. A. Brown, 1992: Effects of radar proximity on single-Doppler velocity signatures of axisymmetric rotation and divergence. *Mon. Wea. Rev.*, **120,** 2798–2807.

Zrnić, D. S., and R. J. Doviak, 1975: Velocity spectra of vortices scanned with a pulse-Doppler radar. *J. Appl. Meteor.*, **14,** 1531–1539.